MINISTRY OF EDUCATION AND TRAINING

VIETNAM ACADEMY OF SCIENCE AND TECHNOLOGY

GRADUATE UNIVERSITY SCIENCE AND TECHNOLOGY

Nguyen Thi Bich Ngoc

THE ROLE OF MAGNETIC FIELDS IN STAR FORMATION

SUMMARY OF DISSERTATION ON SCIENCES OF MATTER

Major: Atomic and Nuclear Physics
Code: 9 44 01 06

Hanoi - 2026

The dissertation is completed at: Graduate University of Science and Technology,
Vietnam Academy Science and Technology

Supervisors:

1. Supervisor 1: Assoc. Prof. Pham Ngoc Diep, Vietnam National Space Center
2. Supervisor 2: Prof. Hoang Chi Thiem, Korea Astronomy and Space Science Institute, University of Science and Technology, Korea

Referee 1:

Referee 2:

Referee 3:

The dissertation is examined by Examination Board of Graduate University of Science and Technology, Vietnam Academy of Science and Technology at…….. (time, date……)

The dissertation can be found at:

1. Graduate University of Science and Technology Library
2. National Library of Vietnam

Preface

1. Motivation

How stars form is one of the most fundamental questions in astronomy. Stars commonly form in dense and cold molecular clouds. Over the past few decades, the general picture of star formation by the gravitational collapse of a dense core within its parent molecular cloud has been studied. However, the star formation rate of the Milky Way is observed to be only about 0.68-1.45 solar masses per year [1], which is about ten times lower than what is predicted by simple models of gravitational collapse [2]. This major discrepancy suggests that gravitational collapse alone cannot account for the low rate of star formation observed throughout the Galaxy. Instead, it highlights the crucial role of additional physical processes, such as magnetic fields, turbulence, and stellar feedback, which act to support molecular clouds against collapse, regulate fragmentation, and limit the conversion of gas into stars. The details of this picture, such as their roles and relative contribution to the process, need to be uncovered. Among them, magnetic fields are crucial in shaping molecular clouds and influencing the subsequent collapse and fragmentation, or guiding and channeling material during the collapse.

Addressing these issues requires better observational constraints on magnetic field morphologies and strengths across various objects with different physical conditions, as well as comparisons with theoretical models. Thanks to advances in modern technology and observational

instruments, particularly the addition of polarimeters to single-dish telescopes such as the James Clerk Maxwell Telescope (JCMT), the Stratospheric Observatory for Infrared Astronomy (SOFIA), and the Atacama Pathfinder EXperiment (APEX), as well as interferometers like the Atacama Large Millimeter/submillimeter Array (ALMA) and NOrthern Extended Millimeter Array (NOEMA), and space-based observatories like *WMAP* and *Planck*, new data have increasingly high spatial resolution and sensitivity. It has enabled us to study magnetic fields at various scales, ranging from galaxies to the interstellar medium, star-forming regions, molecular clouds, and young stars.

Recently, dust-polarized thermal emission has been widely used to study magnetic fields in the star formation process (e.g., [3]) because non-spherical grains tend to align with the ambient magnetic field due to the Radiative Torque (RAT) alignment theory [e.g., 4]. Although the RAT alignment (RAT-A) theory has been successfully tested with starlight polarization [5], observational testing of the RAT paradigm, including RAT-A and RAT Disruption (RAT-D)–a new physical effect discovered by [6] has not been conducted using thermal dust polarization. The RAT paradigm predicts that the alignment of grains with the magnetic field can change depending on the intensity of the stellar radiation, the local gas properties (e.g., density and temperature), and the grain properties (size and composition) [7]. Hence, studying how grain alignment and disruption vary in different regions can shed light on both the properties and fundamental physics of dust, as well as the properties of magnetic fields in star-forming regions.

2. Research Objectives

This PhD thesis aims to study the role and characteristics of magnetic fields and dust physics in star formation. Specifically, this thesis aims to: (1) investigate the role of magnetic fields in star formation by measuring the structure and strength of magnetic fields in molecular clouds and filaments, and (2) test the RAT paradigm using polarization observations and numerical modeling.

I focus on combining polarimetric data from two powerful instruments, JCMT/POL-2 and SOFIA/HAWC+, to study thermal dust polarization in five interesting star-forming regions: Auriga (LkHα 101), M17, G11.11–0.12, Musca, and OMC-1. The diversity of these regions allows us to probe environments with different densities, temperatures, and radiation fields.

3. Main Thesis Contents

This thesis is organized as follows:

Chapter 1: Introduction An overview of the process of star formation and the ISM, and the broader context of magnetic fields and dust in star formation. It also introduces the motivation and objectives of the thesis.

Chapter 2: Far-IR and submm Polarization Observations presents the observational data and instrumentation used in this study. It introduces the target star-forming regions of this thesis, Auriga (LkHα 101), M17, G11.11–0.12, Musca, and OMC-1.

Chapter 3: Magnetic Fields in Star-Forming Regions focuses on the analysis of magnetic fields using polarization data, presents results of magnetic fields, including morphology and strength, and a discussion of the role of magnetic fields in star formation.

Chapter 4: Observational Studies of Grain Alignment and Evolution investigates dust physics and grain alignment mechanisms through observational studies of Auriga, M17, and G11.11–0.12. I examine the variation of polarization fraction with total intensity, dust temperature, and column density, and assess the roles of RAT-A and RAT-D effects. I also evaluate the importance of magnetic field tangling and magnetic relaxation, and present evidence for grain growth in dense environments.

Chapter 5: Numerical Modeling of Thermal Dust Polarization presents numerical modeling of thermal dust polarization based on the RAT paradigm using the `DustPOL-py` code. I apply modeling to Musca and OMC-1 to test the RAT-A and RAT-D effects in these regions.

Chapter 6: Summary and Future Work summarizes the main findings of the thesis, discusses their implications for dust physics and the role of magnetic fields in star formation, and outlines potential studies for future work.

Chapter 1: Introduction

Chapter 1 provides an overview of star formation within its broader astrophysical context, describing interstellar matter, from diffuse gas and dust in the interstellar medium to the formation of dense cores and protostars. Both low- and high-mass star formation scenarios are introduced. The filaments, where most of the star-forming activities take place, are presented. A thorough review of observational methods for the magnetic field, including Zeeman splitting, Faraday rotation, and, particularly, dust polarization, has been conducted. In addition, Chapter 1 introduces interstellar dust, including its composition and size distribution, which are crucial for interpreting polarization observations. The RAT paradigm [e.g., 4, 6] is presented as the leading model, in which anisotropic radiation torques spin up irregularly shaped grains, aligning them with the magnetic field. Radiative Torque Alignment (RAT-A) predicts that the alignment efficiency depends on local conditions, increasing with radiation field strength and decreasing with gas density due to collisional damping. Radiative Torque Disruption (RAT-D) is the mechanism by which, under intense radiation, grains can rotate so rapidly that centrifugal stresses exceed their tensile strength, leading to their fragmentation. Together, RAT-A and RAT-D form the theoretical foundation for the RAT paradigm, which is explored throughout the thesis.

Chapter 2: Far-IR and submm Polarization Observations

Chapter 2 introduces the main observations of this work from polarimetric facilities, including JCMT/POL-2 and SOFIA/HAWC+. Targets include diverse molecular environments: Auriga-California (the LkHα 101 region), M17, G11.11 -0.12 (also known as G11, colloquially referred to as the Snake filament), Musca, and OMC-1, selected to span a range of radiation fields, densities, and evolutionary stages. The ancillary data for studying, including dust temperature, gas column density, and spectral lines, are also presented in this chapter.

The relevant information on their corresponding polarization data used in this thesis is summarized in Table 2.1.

Table 2.1: Information on investigated targets, used facilities, and polarization observations.

Object	Distance pc	Facility	Wavelength μm	Beam size	Representative for
Auriga	466	JCMT	850	$14\farcs6$	Low-mass star formation
M17	1980	SOFIA	154	$13\farcs6$	Photodissociation Region
G11	3600	SOFIA	214	$18\farcs2$	Infrared Dark Cloud
Musca	170	*Planck*	850	$5'$	Simple filament
OMC-1	388	SOFIA	214	$18\farcs2$	High-mass star formation

Chapter 3: Magnetic Fields in Star-Forming Regions

Chapter 3 investigates magnetic field morphologies and strengths across LkHα 101, M17, and G11. Magnetic field strengths are calculated using the Davis-Chandrasekhar-Fermi (DCF) method [8, 9]. The roles of magnetic fields are quantified by considering their relative importance in comparison with other factors, such as gravity via the mass-to-flux ratio, λ, and turbulence through the Alfvénic Mach number, $\mathcal{M}_A$.

This work presents the first measurements of magnetic fields in the LkHα 101 region. The inferred magnetic fields, shown in Figure 3.1, are generally aligned with the filamentary structure in the southwestern dust lane. However, the field displays a more complex configuration in the dense central region (around the star shown in Figure 3.1). The magnetic field strengths estimated using the DCF method are $\sim$91 μG in the central region and $\sim$138 μG along the dust lane. The magnetic energy density dominates over turbulent kinetic energy, as evidenced by sub-Alfvénic conditions ($\mathcal{M}_A \simeq 0.6$). In addition, the central and lane regions are found to be magnetically sub-critical (mass-to-flux ratio $\simeq 0.3$), indicating that magnetic pressure is sufficient to counteract gravitational collapse. These results align with the low star formation efficiency in Auriga [10, 11].

In the M17 region, the magnetic field morphology derived from SOFIA/HAWC+ observations (Figure 3.2) reveals a well-organized, hourglass structure, particularly in the higher-density southern region

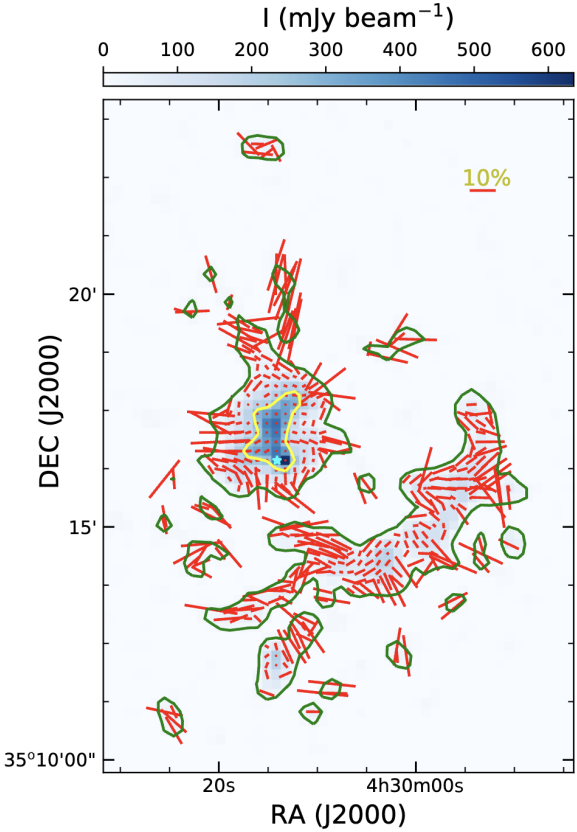

Figure 3.1: Magnetic field orientation (red line segments) toward the LkHα region overlaid on the 850 μm dust continuum intensity map. The length of the line segments is proportional to the polarization degree, $P(\%)$. A 10% line segment is shown for reference. Green contours indicate emission at 15 mJy beam^{-1}, and the yellow contour marks the 250 mJy beam^{-1} level. The B-type star LkHα 101 is indicated by a cyan star.

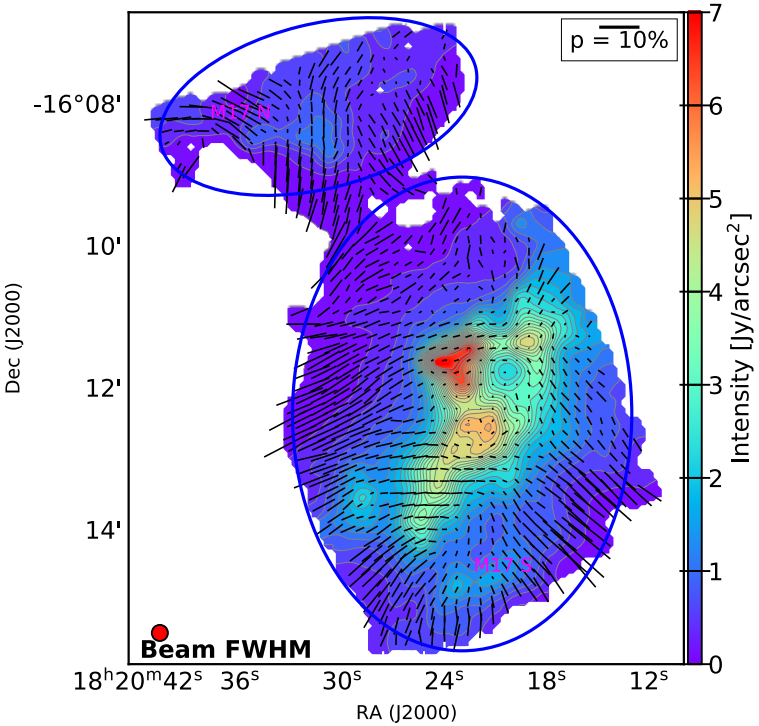

Figure 3.2: Map of the inferred magnetic field orientation in the M17 region observed by SOFIA/HAWC+. The segments are proportional to the polarization percentage with a reference segment corresponding to 10% polarization. The color scale shows the total intensity in units of Jy/arcsec^2. The beam size is shown in the lower left corner. The blue ellipses mark the M17-N and M17-S regions mentioned in the text.

(M17-S). This morphology suggests magnetic field lines being gravitationally dragged inward toward dense central regions. Using the DCF method, the magnetic field strengths are estimated to be 980 ± 230 μG in M17-N and 1665 ± 885 μG in M17-S. The estimated Alfvénic Mach

numbers are sub-Alfvénic ($\mathcal{M}_A < 1$) in both sub-regions, implying that magnetic pressure dominates over turbulent motions. Additionally, the mass-to-flux ratios are found to be sub-critical ($\lambda < 1$), indicating that magnetic fields are sufficiently strong to resist gravitational collapse. These results suggest that magnetic fields play a key role in regulating star formation in M17, particularly by suppressing the formation of stars. This magnetic regulation scenario is consistent with previous findings that there is a deficiency of massive star formation in the region [12].

In the G11.11 -0.12 filament, the magnetic field structure was mapped and shown in Figure 3.3. The inferred magnetic field orientation is predominantly perpendicular to the spine of the filament, as illustrated in Figure 3.4. I applied an updated technique based on the DCF method to compute a magnetic field strength map for the central region of G11, where ancillary data are available for comparison (Figure 3.5, left). The field strengths range from 100 to 600 μG, with the highest values concentrated near the dense spine of the filament and the lower values in the outer regions with lower density. The mass-to-flux ratio map (Figure 3.5, right) indicates that the central region is magnetically sub-critical. Further studies of the present thesis also show that the G11 filament is mainly under sub-Alfvénic conditions. These results suggest that strong, ordered magnetic fields play a central role in supporting the G11 filament against gravitational collapse. This behavior is consistent with the early evolutionary phase of a filament, in which material is still being accreted along magnetic field lines.

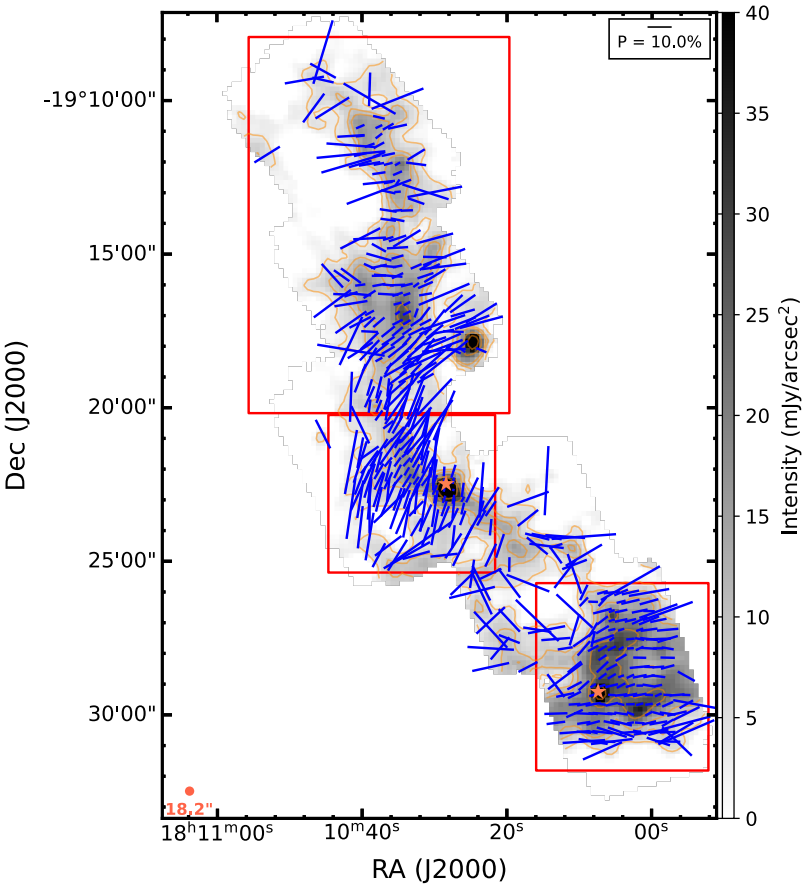

Figure 3.3: Map of magnetic field orientation toward G11 at 214 μm, observed with SOFIA/HAWC+, the length of half-vectors represents the polarization degree. Orange contours correspond to intensity levels of I = 3.6, 8.4, 12.0, 24.0, and 42.0 mJy arcsec^{-2}. The three regions mentioned in the text are defined by the three red rectangles for the North, Center, and South regions, respectively.

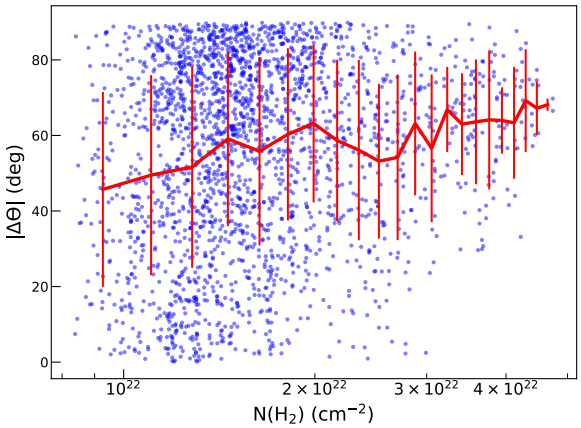

Figure 3.4: Dependence of the angular difference between the magnetic field orientation and the filament spine, $\Delta\Theta$, on column densities. The thick red curve shows the running means of $|\Delta\Theta|$ and the error bars are their RMSs calculated for a bin size of 1.77×10^{21} cm^{-2}.

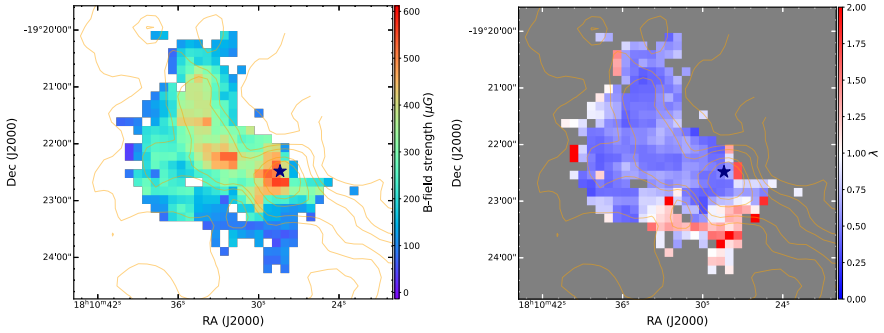

Figure 3.5: Left: Map of magnetic field strengths calculated for each pixel toward the center region of G11. Right: Map of mass-to-flux ratio toward the center region of G11. The dark blue star indicates the location of the massive protostellar candidate (P1). The contours are the same as in Figure 3.3.

Chapter 4: Observational Studies of Grain Alignment and Evolution

Chapter 4 presents a comprehensive analysis of dust polarization observations in Auriga, M17, and G11.11 -0.12 to probe the physics of grain alignment and test the predictions of the RAT-A and RAT-D mechanisms. The Chapter also addresses the long-standing debate surrounding the "polarization hole", a depolarization effect frequently observed in polarization measurements. The depolarization effect can be due to loss of grain alignment, magnetic field tangling, or projection effects (as measured magnetic fields are the 3D magnetic fields projected on the plane of the sky). This effect is the decrease of the polarization fraction toward regions of higher intensity or column density, as illustrated by the length of the half-vectors shown in Figures 3.1, 3.2, and 3.3. It is often analyzed using polarization versus intensity plots, such as in Figure 4.1 (left). The slope of P vs. I, $\alpha \sim 1$, implies a complete loss of alignment in dense cores, while $\alpha < 1$ indicates that the grains are still partially aligned. In Auriga, a slope of ~0.82 suggests a reduced alignment efficiency in the denser region. M17 shows a shallower slope ($\alpha = 0.51$), consistent with a higher alignment efficiency under the influence of strong radiation fields. In G11, steeper slopes ($\alpha \approx 0.80$–0.93) indicate significant depolarization toward the quiescent filament spine with a lack of embedded stars.

Interestingly, in the LkHα 101 region, the polarization fraction is observed to decrease sharply toward the B star, LkHα 101 (see Fig-

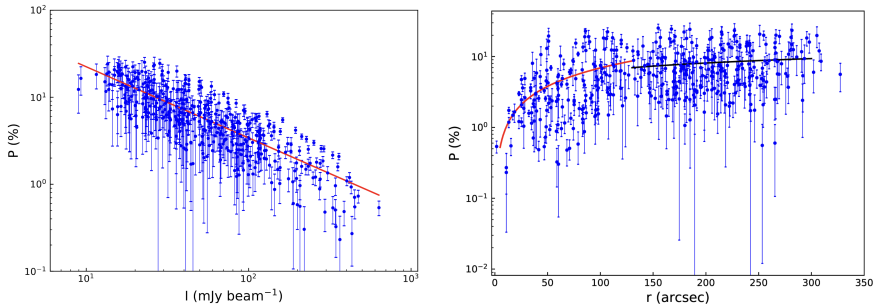

Figure 4.1: Left: Dependence of polarization fraction on the total intensity. P tends to decrease with increasing I. The solid line is the best fit to a power law function. Right: Dependence of P on r. The r-dependence of P is fitted to a power law function for $r < 130''$ (red curve) and $r > 130''$ (black curve).

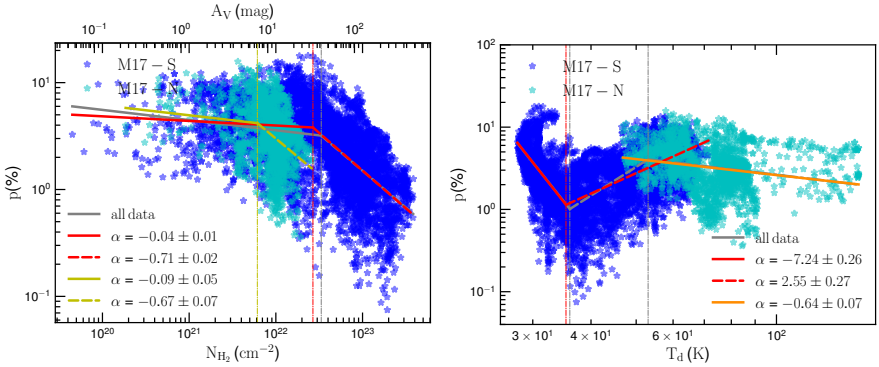

Figure 4.2: Left: The relationship between polarization fraction and column density. Right: the relationship between polarization fraction and temperature. In both panels, α is the index of the best-fitting power-law model.

ure 4.1, right), despite the increasing radiation field. This behavior contradicts the standard prediction of RAT-A, which expects a higher

degree of grain alignment in stronger radiation fields. The observed trend could be explained by RAT-D. Other effects, such as the geometry of the magnetic fields and turbulence, may also contribute to explaining the polarization hole in this region. In the southern region of M17 (M17-S), polarization decreases with the column densities (Figure 4.2, left), consistent with RAT-A, suggesting that the alignment efficiency is reduced in dense regions where radiation is attenuated and collisional damping is stronger. In M17-N, the polarization fraction decreases with increasing dust temperature (Figure 4.2, right), despite the fact that the gas is relatively diffuse. RAT-A cannot explain this polarization pattern. In addition, magnetic field tangling remains largely unchanged in the high dust temperature region (>90 K); therefore, the decrease in polarization percentage cannot be attributed to magnetic field tangling, and this provides observational evidence for the RAT-D effect.

In G11, grain growth in the filament spine is inferred from the polarization slope (α ~0.8–0.9 < 1), which means that the grains in the region are still aligned and require maximum grain sizes larger than the alignment size threshold ~0.3 μm. The calculated threshold is larger than the maximum grain in the interstellar medium, ~0.25 μm (as described by the Mathis-Rumpl-Norsieck distribution [13]). Based on the magnetic field strengths, the magnetic relaxation calculated by MRAT yields high values, which can enhance alignment efficiency. The combined effect of RATs and MRAT can explain the high polarization fraction ($P \geq 20\%$) observed in the outer parts of the filament.

Chapter 5: Numerical Modeling of Thermal Dust Polarization

Chapter 5 presents numerical modeling of thermal dust polarization using the DustPOL-py code to test the predictions of the Radiative Torque paradigm, incorporating both RAT-A and RAT-D mechanisms. The modeling is applied to two well-studied and distinct filaments, Musca and OMC-1 (Figure 5.1). Before constructing the model, I first analyzed the observed polarization fraction trends in these regions in relation to local environmental conditions, including dust temperature, gas density, and magnetic field tangling.

In Musca, a quiescent and simple filament, the observed decrease in polarization fraction toward the denser spine is well reproduced by RAT-A alone. The modeling shows that grain alignment efficiency declines (Figure 5.2, upper panel) with increasing column density due to reduced radiation field and enhanced collisional damping. The model result successfully reproduces the observed polarization fraction from the outer to the inner filament (Figure 5.2, lower panel), confirming that RAT-A can explain the depolarization effect in the low-radiation environment of the filament.

In contrast, OMC-1 is an active star-forming region located in a high-radiation environment. RAT-A alone cannot explain the observed $P - T_{\rm d}$ trends. The polarization fraction is found to first increase with dust temperature, then decrease beyond ~65 K. This increase-decrease trend is a signature of RAT-D, where large grains are disrupted by

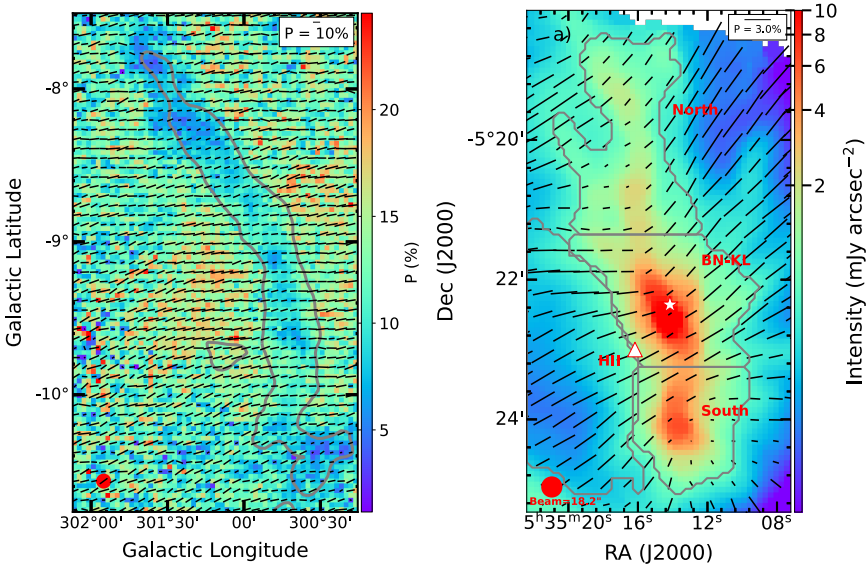

Figure 5.1: Left: Magnetic field orientation map of Musca observed by *Planck*. The length of the line segment is proportional to the polarization fraction P with a 10% reference. Right: Magnetic field orientation map of OMC-1 observed at 214 μm wavelength by SOFIA/HAWC+. The black lines show the orientation of the magnetic field half-vector and are overplotted on the intensity map. Three regions, North, BN-KL, and South, are labeled.

high radiation intensities, reducing the number of aligned grains. The `DustPOL-py` code, which includes both alignment, disruption effects, and magnetic field fluctuations, can reproduce the observed $P - T_{\rm d}$ and $P - N(\rm H_2)$ (polarization hole), shown in Figure 5.3. The "ideal" polarization model (blue and orange lines) cannot reproduce the data (black lines), but the realistic polarization model (red line) considering

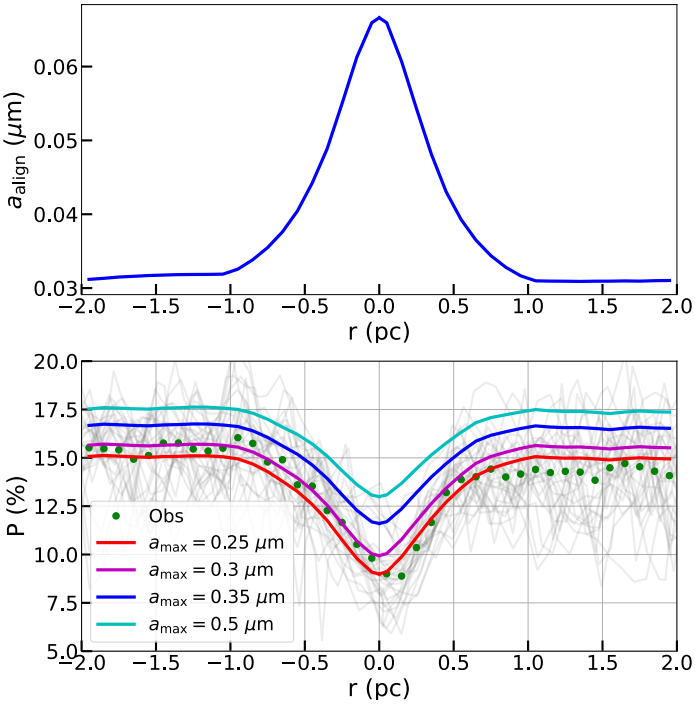

Figure 5.2: Musca. Upper: Minimum alignment size by RATs calculated from our model for Musca. Lower: Comparison of the polarization fraction from our model (thick solid lines) with observation data. The gray curves show P versus r for radial cuts along the filament's spine from observational data. Green dots represent the mean values of the observational P at a certain value of r (distance from the filament's spine). The color curves show polarization fractions from our model with different $a_{\rm max}$. The rapid increase in alignment size toward the filament's spine results in a decrease in the model polarization fraction, successfully reproducing the observed polarization hole.

RAT-A, RAT-D, and magnetic field tangling ($P_{\rm mod}$) can best reproduce the observed variation of $P - T_{\rm d}$ and $P - N(\rm H_2)$ (see Section 5.4.2 for more detail). The successful validation of the RAT paradigm through pixel-by-pixel modeling of polarization emission compared with observational data for two contrasting cases -a quiescent (Musca) and an active star-forming (OMC-1) clouds- offers an approach to test the RAT framework and constrain properties of dust grains in a broader range of astrophysical environments.

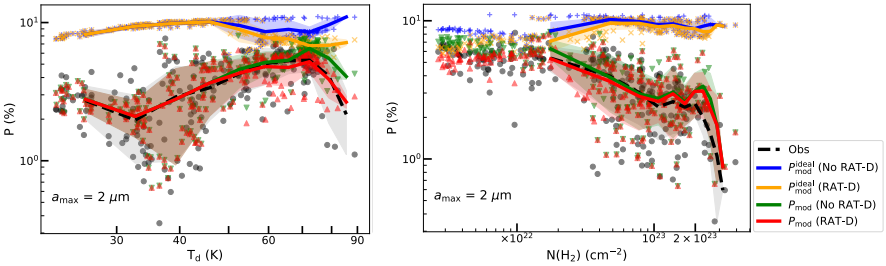

Figure 5.3: OMC-1. Upper: Comparison of the polarization degree versus dust temperature relation from our models (color lines) with observational data (black line). Lower: $P - N(\rm H_2)$ relation. The shaded area represents the 1-σ deviation of each bin of data points, which are shown by points (black for observation data and color for model data).

Chapter 6: Summary and Future Work

Finally, Chapter 6 presents the main findings of the thesis and discusses future directions. Magnetic field structures and strengths were studied in detail in LkHα 101, M17, and G11.11 -0.12, showing that magnetic fields can dominate over gravity and turbulence. The analysis of polarization data under the framework of RAT showed that RAT-A is consistent with the reduced alignment efficiency in dense and low-radiation regions (e.g., Musca, G11); RAT-D can account for the decrease of polarization fraction due to grain disruption in high-radiation environments (e.g., M17, OMC-1, LkHα 101). Evidence of grain growth and enhanced alignment efficiency due to magnetic relaxation was found in G11. Numerical modeling with `DustPOL-py` successfully reproduced the observed polarization trends for Musca and OMC-1.

The analysis techniques developed in the current thesis, in particular for analysing polarization data and pixel-by-pixel modeling, have been first applied to Musca and OMC-1, showing their effectiveness. The approach has been applied to other regions by our international collaborators, especially with the BALLAD-POL project [14, 15, 16]. Future work will focus on expanding to an even broader range of spatial scales, particularly at the core scales, incorporating multi-wavelength polarimetry, and exploring the three-dimensional structure of magnetic fields, which will improve our understanding of properties of dust grains and the role of magnetic fields in star formation.

Bibliography

[1] Thomas P. Robitaille and Barbara A. Whitney. The Present-Day Star Formation Rate of the Milky Way Determined from Spitzer-Detected Young Stellar Objects. *ApJ*, 710(1):L11–L15, 2010.

[2] Christopher F. McKee and Eve C. Ostriker. Theory of Star Formation. *ARA&A*, 45(1):565–687, 2007.

[3] K Pattle and L Fissel. Submillimeter and Far-infrared Polarimetric Observations of Magnetic Fields in Star-Forming Regions. *Front. Astron. Space Sci. Sciences*, 6:15, 2019.

[4] A. Lazarian and T. Hoang. Radiative torques: analytical model and basic properties. *MNRAS*, 378(3):910–946, 06 2007.

[5] BG Andersson, A Lazarian, and John E Vaillancourt. Interstellar dust grain alignment. *ARA&A*, 53:501–539, 2015.

[6] T. Hoang, Le Ngoc Tram, Hyeseung Lee, and Sang-Hyeon Ahn. Rotational disruption of dust grains by radiative torques in strong radiation fields. *Nature Astronomy*, 3:766–775, May 2019.

[7] Le Ngoc Tram and Thiem Hoang. Recent progress in theory and observational study of dust grain alignment and rotational disruption in star-forming regions. *Front. Astron. Space Sci. Sciences*, 9:923927, 2022.

[8] Leverett D. The strength of interstellar magnetic fields. *Phys. Rev.*, 81(5):890, 1951.

[9] Subrahmanyan Chandrasekhar and Enrico Fermi. Problems of gravitational stability in the presence of a magnetic field. *ApJ*,

118:116, 1953.

[10] Hannah Broekhoven-Fiene, Brenda C Matthews, P Harvey, et al. The jcmt gould belt survey: A first look at the auriga–california molecular cloud with scuba-2. *ApJ*, 852(2):73, 2018.

[11] Enrique Vázquez-Semadeni, Alejandro González-Samaniego, and Pedro Colín. Hierarchical star cluster assembly in globally collapsing molecular clouds. *MNRAS*, 467(2):1313–1328, 2017.

[12] Quang Nguyen-Luong, Fumitaka Nakamura, Koji Sugitani, Tomomi Shimoikura, Kazuhito Dobashi, et al. Large-scale molecular gas distribution in the m17 cloud complex: Dense gas conditions of massive star formation? *ApJ*, 891(1):66, 2020.

[13] John S Mathis, William Rumpl, and Kenneth H Nordsieck. The size distribution of interstellar grains. *ApJ*, 217:425–433, 1977.

[14] Saikhom Pravash, Archana Soam, Pham Ngoc Diep, et al. BALLAD-POL. III. Grain Alignment and Disruption Mechanisms in G34.43+0.24 Using Polarization Observations from JCMT/POL-2. *ApJ*, 981(2):128, 2025.

[15] Saikhom Pravash, Thiem Hoang, Archana Soam, et al. BALLAD-POL: IV. Grain alignment mechanisms in Cocoon Nebula (IC 5146) using polarization observations from JCMT/POL-2. *arXiv e-prints*, page arXiv:2507.07205, 2025.

[16] Sadhana Singh, Thiem Hoang, Pham Ngoc Diep, Nguyen Bich Ngoc, and Woojin Kwon. Magnetic Field and Dust Grain Alignment in Serpens Main. In *AAS Meeting*, volume 245 of *AAS Meeting*, page 174.03, 2025.

LIST OF THE PUBLICATIONS RELATED TO THE DISSERTATION

1. **Observations of magnetic fields surrounding LkHα 101 taken by the BISTRO survey with JCMT-POL-2**
   Nguyen Bich Ngoc and BISTRO collaboration, 2021,
   The Astrophysical Journal, 908(1), p.10. DOI:
   10.3847/1538-4357/abd0fc
2. **Studying Magnetic Fields and Dust in M17 Using Polarized Thermal Dust Emission Observed by SOFIA/HAWC+**
   Thuong Duc Hoang, **Nguyen Bich Ngoc**, Pham Ngoc Diep, Le Ngoc Tram, et al., 2022, ApJ, 929, 27. DOI:10.3847/1538-4357/ac5abf2
3. **B-fields And dust in interstelLar fiLAments using Dust POLarization** (BALLAD-POL): I. The massive filament G11.11 -0.12 observed by SOFIA/HAWC+
   Nguyen Bich Ngoc, Pham Ngoc Diep, Thiem Hoang, Le Ngoc Tram, et al., 2023,
   The Astrophysical Journal, 953(1), p.66. DOI:
   10.3847/1538-4357/acdb6e
4. **B-fields And dust in interstelLar fiLAments using Dust POLarization (BALLAD-POL): II. Testing the Radiative Torque Paradigm in Musca and OMC-1**
   Nguyen Bich Ngoc, Thiem Hoang, Pham Ngoc Diep, and Le Ngoc Tram, 2024,
   The Astrophysical Journal, 974(1), 118. DOI:
   10.3847/1538-4357/ad6a5e